Effectiveness of photodecomposition of rhodamine B and malachite green upon coupled tricomponent TiO_2(Anatase-Rutile)/ZnO nanocomposite

Dongfang Zhang

College of Science, Huazhong Agricultural University, Wuhan 430070, PR China
zdfbb66@aliyun.com

Abstract: In this study, mixed phase ZnO-TiO_2 nanocomposite consisting of hexagonal ZnO and anatase/rutile TiO_2 has been synthesized via sol-gel process.The physical and photochemical properties of samples were characterized by X-ray diffraction (XRD), transmission electron microscopy (TEM), UV-vis diffuse reflectance spectroscopy (UV-vis DRS), photoluminscience spectra (PL) and and photocurrent action spectra techniques. In the case of minerlization of rhodamine B (RhB) and malachite green (MG) dyes, the coupled ZnO-TiO_2 nanocomposite with the suitable band structure and the lowest photoluminescence intensity showed the best photodecolorization activity. Synergistic effects between the two oxides for photocatalytic decomposition of RhB and MG are proposed to elucidate the decolorization mechanism. The lifetime of electrons and holes was prolonged in the ZnO-anatase/rutile multiple-component system, which can enhance the light harvest and the ability of generating photo-induced electron-hole pairs of active sites, and the favorable electron-transfer properties in the coupled ZnO-TiO_2 nanocomposite. Therefore, the as-prepared ZnO-TiO_2 nanocomposite showed an excellent efficiency towards the removal of aqueous organic dyes and it is of certain significance for environmental photocatalysis.

Keywords: Photocatalytic, heterostructure, dyes

Introduction

With the development of technology, the environmental pollution deriving from artificial products has become a serious problem. There is a considerable need for the removal of color from wastewater/effluents. The discharge of dye-bearing wastewater into natural streams and rivers from the textile, paper, carpet, leather, distillery and printing industries poses severe problems, as dyes impart toxicity to aquatic life and are damaging to the aesthetic nature of the environment. Many of the dyes used in these industries are stable to light and oxidation, as well as being resistant to aerobic digestion. Therefore, color bearing effluents need to be treated to remove the hazardous dye in an economical fashion and to the prescribed concentration levels before they are discharged into bodies of water. The treatment of highly colored wastewater containing hazardous industrial chemical effluents is one of the growing needs of the present time. In response to this, materials which can remove the harmful pollutants irreversibly and eliminate them completely have been developed [1–10].

Heterogeneous photocatalysis is an emerging technique for environmental remediation, where semiconductor materials are used as photocatalysts [11–26]. When organic pollutants are decomposed by heterogeneous catalytic reactions, the pollutant molecules are adsorbed on the surface of the catalysts, where chemical bonds are broken and formed, and eventually small organic molecules or carbonate are released as decomposed products. Thus, advanced oxidation processes (AOP) have been extensively investigated with regard to the degradation of pollutants [27–34]. In particular, heterogeneous photocatalysis appears today as an interesting application of AOP, and leads to a complete mineralization of most organic compounds. In this process, hydroxyl radicals $HO^{\cdot}$ are generated when the photocatalyst is illuminated in the presence of water and air. These ultra-reactive species associated with oxygen are able to achieve a complete mineralization of organic pollutants into carbon dioxide, water and other non-toxic products [35–39]. Among various semiconductor photocatalysts for environment purification, titania appears to be the most promising and important one due to its stable physical and chemical characteristics, unique electronic properties, strong oxidizing power, non-toxicity and low price [40–45]. However, the wide band gap of TiO_2 (>3.0 eV) and the high recombination rate of the photoinduced electron-hole pairs formed in photocatalytic processes limit the efficiency of the photocatalytic degradation of toxicants. Therefore, it is desired to improve photocatalytic activity. Coupling two semiconductor nanoparticles with different band gap widths has been demonstrated as one of the most effective ways to enhance the photocatalytic efficiency of the single one [46–53]. There have been some studies on the

improvement of photocatalytic performance of TiO_2 coupled with metal oxide [54, 55]. The results showed that coupled semiconductor photocatalysts was a novel alternative to achieve a more efficient charge separation, an increased lifetime of the charge carriers, and an enhanced interfacial charge transfer to adsorbed substrates. At the same time, their physical, electronic and optical properties are greatly modified [56]. It is generally accepted that properties of composite obtained via chemical synthesis often cannot be considered as a simple superposition of the properties of individual components due to the strong surface interactions between the closely packed nanoparticles in the binary oxide systems [57].

Although TiO_2 has proven to be one of the best photocatalysts for decomposing organic compounds, with uses in self-cleaning glass and photo-induced water splitting, ZnO nanomaterials have also been demonstrated to be efficient photocatalysts for the decomposition of organic components due to its large exciton binding energy [58]. The biggest advantage of ZnO is that it can absorb a larger fraction of UV spectrum and the corresponding threshold of ZnO is 425 nm [59]. Coupling two semiconductor nanoparticles with different electronic structures has been verified to promote the separation efficiency of photogenerated charges and extended the range of excite spectrum [60]. The modification of the electronic properties of the coupled semiconductor with respect to the single ones is invoked to explain the photocatalytic behavior on specific nanoscale material. It is thus speculated that the nanocomposites composed of ZnO and TiO_2 exhibit useful applications in photocatalysis. Therefore, it is necessary to examine the applicability of TiO_2/ZnO binary oxide systems for the photocatalytic degradation of organic pollutants and enrich current knowledge on the subject and certain behavior in other kinds of photoreactions take place in the liquid-solid regime.

This scientific work addresses a topic of great interest that, after a while, it remains one of the great challenges to be solved by the researchers involved in heterogeneous photocatalysis, as it is to broaden the active spectrum of TiO_2 for a better exploitation of the natural light for solar photocatalytic applications. This paper describes an investigation of the use of TiO_2/ZnO nanocomposite in the photodecomposition of harmful dyes. It is claimed that the anatase/rutile TiO_2 and hexagonal ZnO mixed composite system are very effective for the photodecomposition of organic dyes. The synergistic effect make the dye molecules be completely decomposed or decolorized within tricomponent system. The relationship between the nanoscale structure of composite systems and the corresponding photoelectrochemical properties was also explored and addressed for understanding the underlying properties. The effect and the advantage of the combination of TiO_2 and ZnO on the character and the resultant their photocatalytic activity were described compared with TiO_2 alone, especially in the photoabsorption, the photoemission and the photocurrent measurements in order to make the effect of the combination of TiO_2 and ZnO more clear. The unique charge-transfer phenomenon increases the availability of the electron-hole pairs on the surface of the photocatalyst and thus an improvement of the occurrence of redox processes with species adsorbed on the surface of the catalyst or a higher reaction rate can be expected.

Experimental

Most of the reagents were purchased from Shanghai Chemicals Co. Ltd. with analytic grade and used as received without further purification. Distilled water was employed throughout in all experiments. Commercial ZnO (Merck, 99 % purity) was used as received throughout the experiments. The nanostructured ZnO-TiO_2 composites were prepared by means of sol-gel method. In a typical synthesis process for the preparation of ZnO-TiO_2 composite nanopowders, titanium-(IV)-isopropoxide, and deionized water (as hydrolysis agent) were mixed in absolute ethanol with hydrochloric acid (HCl, Merck, 37 %) in terms of molar ratio of Ti : C_2H_5OH : H_2O : HCl = 1 : 10 : 6 : 0.2 under vigorously stirring in order to form sols. Then a desired amount of ZnO was added into the above mixture solution with Ti/Zn molar ratio of 1.2 : 1.0. After aging for 6—13 h, the sols transformed into gels. Then the gels were in sequence dried, ground in a ball mill, and pretreated at 80 °C for 3.0 h. Finally, the obtained xerogel precursor was annealed at 600 °C for 2.0 h to obtain the catalyst used in this study. In order to compare the results, nanometer anatase TiO_2 (ST-01, made from Ishihara-Sangyo Co. Ltd, Japan, crystallite size is about 20 nm) as a commercially available photocatalyst was also applied in the photocatalytic test to evaluate the effectiveness of decolorization of the dye solution.

X-ray powder diffraction (XRD) data were recorded at room temperature with an X-ray diffractometer (XRD-6000, Shimadzu Corporation) using Cu Kα irradiation (λ = 0.15408 nm), operated at 40 kV and 100 mA, which was used to identify the crystallographic information such as structure properties, chemical composition and phases of the products.

The size and morphology of the acquired samples are characterized by transmission electron microscopic. The observations and recording of images were performed with a HITACHI H-7650 transmission electron microscope at 80 kV and a Gatan 832 CCD camera. The percentage of UV-vis reflectance was measured by diffuse reflectance spectroscopy (DRS) for the powder form of the catalysts using a scanning UV-vis-NIR spectrophotometer (Varian Cary 500) in the region of 200—800 nm. The spectrophotometer was equipped with an integrating sphere assembly and polytetrafluoroethylene was used as a reflectance material. The reflectance data were converted to the absorbance values, F(R), based on the Kubelka-Munk theory. The photoluminescence (PL) emission spectra of the samples were measured with a RF-5301 PC spectrofluorophotometer (Shimadzu Corporation) by using the 320 nm line of a Xe lamp as excitation source at room temperature. The synthesized TiO_2/ZnO nanocomposite or ST-01 TiO_2 paste for the fabrication of a photoanode was obtained by mixing 5 mL of ethanol and 250 mg of TiO_2/ZnO nanocomposite or ST-01 TiO_2 powder homogeneously. The obtained paste was spread on the FTO conducting glass with a glass rod, using adhesive tapes as spacers. After the films were dried under ambient conditions, they were sintered in air at 600 °C for 2 h. The film thickness measured to be about 0.002 mm. Photocurrent action spectra were measured in a two-electrode configuration home-built experimental system, where the sintered photoanode served as the working electrode with the active area of about 1 cm^2 by using Teflon tape and a platinum wire was used as the counter electrode. A 500 W Xe lamp with a double-prism monochromator was used as the light source. The generated photocurrent signal was collected by using a lock-in amplifier (SR830 DSP) synchronized with a light chopper (SR540).

Photocatalytic efficiency of the as-prepared systems was estimated in terms of the degradation of RhB or MG aqueous solution. Rohdamine-B (RhB), a xanthene dye, is widely used as a colorant in textiles and food stuffs, and also a well-known water tracer fluorescent. RhB is harmful if swallowed by human beings and animals, and causes irritation to the skin, eyes and respiratory tract. The artificial light photocatalytic activity test is conducted in a quartz photoreactor with a cylindrical configuration. Photoirradiation was carried out by employing a 500 W halogen lamp (a 400 nm cutoff filter was placed above the reactor to cutoff UV light) placed inside the photoreactor which emitted irradiation comparable to sunlight. The distance between the surface of reaction solution and light source is adjusted to about 15 cm. A certain amount of photocatalyst powder (25 mg) is added to 150 ml aqueous Rohdamine-B (1.0×10^{-5} mol/L) solution. Before the occurrence of the photocatalytic degradation, the suspension is magnetically stirred in the dark for 30 min to saturate the adsorption of Rohdamine-B dye on photocatalyst surface as a reference point. The photocatalytic decomposition of RhB aqueous solution was characterized by a UV-visible spectrometer based on the Beer-Lambert law. During the irradiation experiments, aliquots (5 ml) are withdrawn from the suspension at regular time intervals and are immediately centrifuged at 6000 rpm for 20 min to remove solids. The concentration of Rohdamine-B after illumination is monitored at λ = 553 nm using UV-vis spectrophotometer (Spectrumlab 2450, Shimadzu Corporation). The degradation rate of the Rohdamine-B can be determined by the formula: $X\,[\%] = (A_0 - A_t)/A_0 \times 100$ %, where A_0, A_t represents the initial absorbance and the absorbance of the aqueous RhB after a certain period of illumination time t, respectively. The degradation experiment also be done for MG dye using the similar method.

Results and Discussion

Fig. 1 shows the XRD patterns for commercial TiO_2 nanoparticles (ST-01) and ZnO-TiO_2 composites obtained after calcinations at 600 °C, which provide further insight into the crystallinity of the products. The peaks are identified and assigned referring to the JCPDS data (Powder Diffraction Card, #21-1272 for TiO_2 (anatase), #21-1276 for TiO_2 (rutile), #36-1451 for ZnO, #26-1500 for $ZnTiO_3$). For the commercial TiO_2 nanoparticles (ST-01) as received, all diffraction peaks can be well indexed as phase-pure anatase TiO_2. The diffraction peaks located at 2Θ = 25.2 ° (101), 37.8 ° (104), 47.9 ° (200), 53.9 ° (105), 55.0 ° (211), 62.5 ° (204), 68.7 ° (116), 70.4 ° (220) are perfectly indexed to the anatase TiO_2 phase (as displayed in Fig. 1a). However, it can be found that wurtzite ZnO phase is existent in the calcined ZnO-TiO_2 composites at 600 °C. The peaks located at 2Θ = 36.1 ° (101), 47.9 ° (102), 56.5 ° (110), 63.0 ° (103) are characteristic diffraction peaks of the ZnO crystallites confirmed by a search-match database analysis, suggesting the formation of hexagonal crystalline phase composite of wurtzite. Moreover, new diffraction peaks located at 2Θ = 27.4 ° (110), 36.1 ° (101), 41.2 ° (111), 54.2 ° (211), 56.8 ° (220) indicate the formation of rutile TiO_2 at a calcinations temperature of 600 °C. Compared with the monocomponent nanomaterials (commercial TiO_2 nanoparticles, ST-01), the coupled nanocomposites indeed consist of both anatase or rutile TiO_2 and wurtzite ZnO, which is

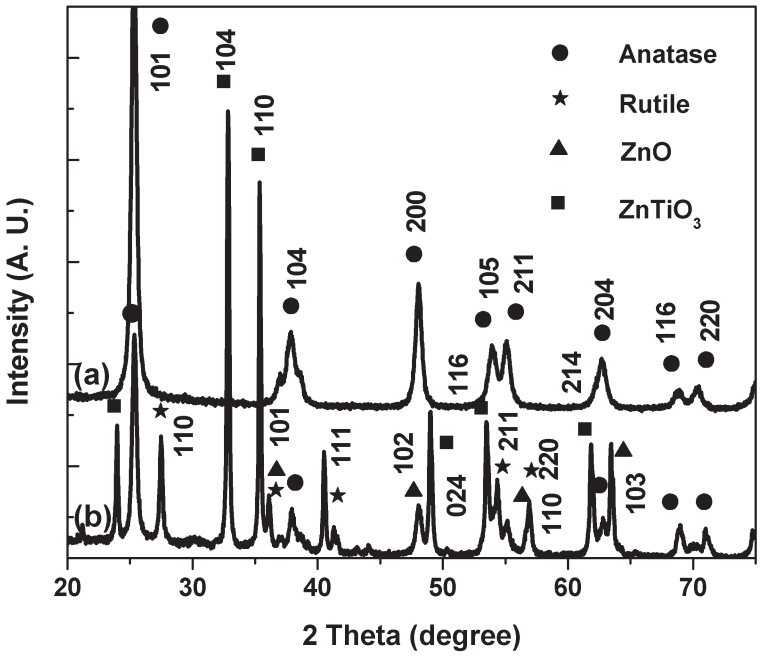

Fig. 1. X-ray diffraction patterns of different samples: (a) Commercial TiO_2 (ST-01) and (b) ZnO-TiO_2 nanocomposite.

evidently shown in the XRD pattern. Besides, the appearance of diffraction peaks located at 2Θ = 32.7 ° (104), 35.2 ° (110), 49.0 ° (024), 53.5 ° (116), 61.8 ° (214) confirms the generation of ecandrewsite $ZnTiO_3$ phase (see Fig. 1b). The reaction between TiO_2 and ZnO to form $ZnTiO_3$ at 600 °C is expressed as follows: ZnO + TiO_2 → $ZnTiO_3$. Actually, a considerable amount of wurtzite ZnO may be induced as solute in TiO_2 to form TiO_2-base binary solid solution. In XRD pattern of composite sample prepared at 600 °C, ZnO-TiO_2 solid solution reaches the proper stiochiometric ratio to form hexagonal phase of $ZnTiO_3$. The rutile and anatase contents in the composite sample can be estimated using the Spurr equation:

$$M_R = \frac{1}{1 + 0.8\,[I_A(101)/I_R(110)]} \times 100 \qquad (1)$$

$$M_A = 100 - \frac{1}{1 + 0.8\,[I_A(101)/I_R(110)]} \times 100 \qquad (2)$$

where M_R and M_A are, respectively, the mass fraction of rutile and anatase in the composite sample and I_R and I_A are the integrated intensities of the main peaks of rutile (110) and anatase (101), respectively. The phase content of the prepared ZnO-TiO_2 composite is thus determined to be A(58.8 %)/R(41.2 %). Average crystallite size of ZnO-TiO_2 composite photocatalyst was estimated according to Scherrer's equation [61, 62], $d = k\lambda/(b\cos(2\Theta))$, where d was the average crystallite size (nm), λ was the wavelength of the Cu-Kα applied (λ = 0.15406 nm), Θ was the Bragg's angle of diffraction, b was the full-width at half maximum intensity of the peak and k was the constant usually applied as 0.89. The average crystallite size of ZnO-TiO_2 composite photocatalyst with Ti/Zn molar ratio of 1:1 was estimated to be 32.0 nm. The microstructure of the obtained samples were further identified by transmission electron microscopy (TEM) imaging technique to get the information about particles size, morphology and number density, and the results were shown in Fig. 2. As can be seen, the TEM image shows that the ZnO-TiO_2 power consist of irregular particles around 20—35 nm. Due to aggregation, ZnO-TiO_2 composite contains different size particles with irregular round shape, and the primary TiO_2 particles have nonuniform diameters ranged from 20—40 nm forming a dense structure with a relatively smooth surface, whereas the spherical-like particles corresponded to the zinc oxide were randomly dispersed into the titania particles. The observation from the TEM graph was basically consistent with the average crystallite size estimated from XRD analysis, and usually TiO_2 grains are inclined to grow bigger more easily without any addition of foreign species.

The photocatalytic efficiency of ZnO-TiO_2 composite system is highly related to their light absorption including amount, wavelength range, and absorption peak absorption. To characterize the absorption properties of modified photocatalyst, diffuse reflectance (DR) measurement was carried out and then data were converted into the equivalent absorption coefficient using the Kubelka-Munk method [63]. As is shown in Fig. 3, the curve of commercial TiO_2 (ST-01) has strong light absorption

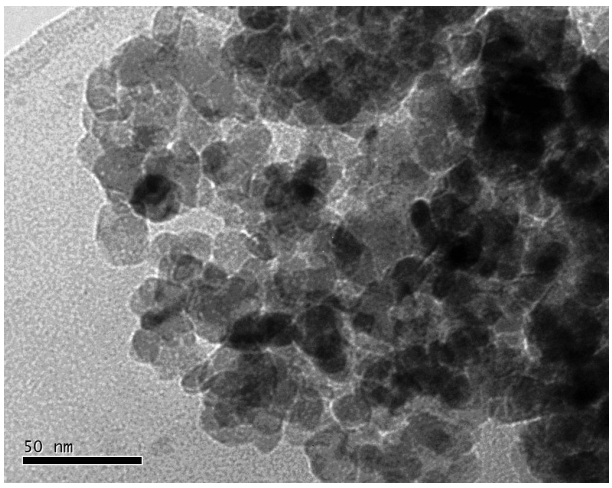

Fig. 2. A representative TEM image of the as-synthesized ZnO-TiO_2 nanocomposite.

property at the wavelength shorter than 400 nm, and the absorption edge appears at about 375 nm, which is in line with the well-known fact that the band-gap of anatase TiO_2 is approximately 3.2 eV, and thus ST-01 TiO_2 can not be excited by photons with wavelengths beyond 400 nm. According to the energy band structure of TiO_2, the optical absorption in the UV region is mainly attributed to the electron transitions from the valence band to conduction band (band-to-band transition, O2p → Ti3d). The absorption edge of commercial anatase TiO_2 appears blue-shift slightly compared to the bulk TiO_2. This blue shift and increment in band gap may attribute to the size-quantization effect [64]. However, the as-prepared ZnO-TiO_2 composite system gave a broad absorption band in the visible region, which is an indication that the composite catalyst can absorb lights in the longer wavelength range, and therefore it can more efficiently utilize visible lights for the photocatalytic purpose. As suggested by the XRD of ZnO-TiO_2 catalyst, the Ti-O-Zn bonding for $ZnTiO_3$ crystallites is already formed in the composite system. Such formation might induce defects to the crystal lattice structure of anatase TiO_2, resulting in an increasing of the absorption edge in comparison to the neat TiO_2. Because of the absorption wavelength range red-shift greatly and absorption intensity increases for wavelength λ > 370 nm, the formation rate of electron-hole pairs on the ZnO-TiO_2 composite catalyst surface also increases greatly, resulting in the photocatalyst exhibiting higher photocatalytic activity. The reason for the absorption wavelength range red shifts of the ZnO-TiO_2 composite could probably be attributed to the formation of defect energy level during the binary solid-solution reaction process. Therefore, the as-prepared ZnO-TiO_2 composite inherently possesses the photocatalytic potential for the uphill reactions involved in organic pollutant degradation under UV-Vis region and might be an ideal photocatalyst for the full use of visible light source.

As is well known, the photocatalytic process is initiated by the illumination of a semiconductor

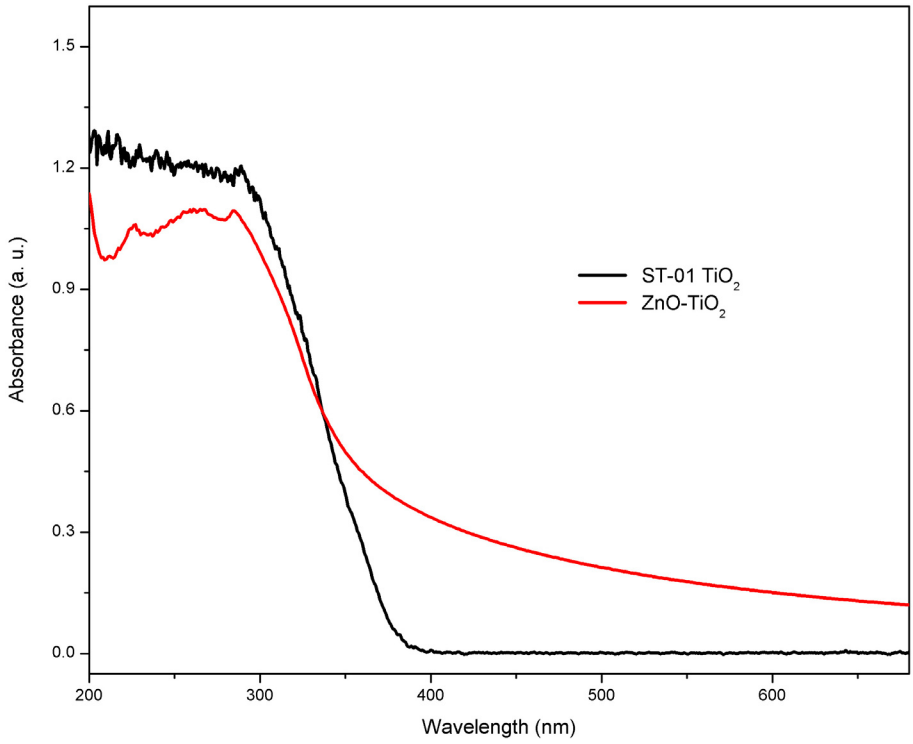

Fig. 3. UV-visible absorption spectra of the as-prepared samples.

catalyst with photon energy greater than the band gap energy of the semiconductor. This irradiation makes photocatalysts release electrons (e^-) and holes (h^+) in the conduction band (CB) and valence band (VB), respectively. The electron-hole pairs formed may recombine in the bulk lattice or migrate to the surface where they can react with the adsorbates. The photogenerated holes migrate to the interface and react with OH^- adsorbed onto the catalyst to create hydroxyl radicals ($OH^\cdot$). The $OH^\cdot$ radicals have extremely strong oxidizing properties and are able to decompose dye molecule. The probability to decompose is then linked to efficiency of hole generation, hole mobility, transport phenomena, and so on. During the process of de-excitation, recombination of some electrons and holes can occur spontaneously driven by electrostatic force and thus the system may release energy in the form of fluorescence emission. Lower fluorescence emission intensity associated with the lower electron-hole recombination rate and vice versa. Fig. 4 displayed the PL spectra of commercial TiO_2 (ST-01) and ZnO-TiO_2 composite. A xenon UV-vis-near-IR excitation lamp was used to excite sample at 320 nm. As can be seen, commercial TiO_2 (ST-01) sample exhibited the highest PL emission band at 350-600 nm. The emission peaks at around 405 nm (3.06 eV) and 446 nm (2.8 eV), showing indirect band gap characteristics [65]. The PL emission could be attributed to the surface state such as Ti^{4+}-OH, when excited with light having energies larger than the band gap of the samples [66]. It is obvious that the relative intensity of the emission spectra of ZnO-TiO_2 composite system is the lower than the unmodified TiO_2, indicating a low recombination rate of electrons and holes. The slower recombination rate will favor to the photocatalytic reaction and maintain the stability of quantum efficiency throughout the reaction process. Therefore, coupling TiO_2 with ZnO is helpful to suppress the recombination of charge carriers and improve the photocatalytic oxidation activity.

In order to examine the structure-specific photoelectrochemical (PEC) properties of the prepared nanomaterials, measurements of the photocurrent action spectra were performed in a home-built PEC experimental system. The photo currents of the bulk and the thin film are also strongly affected by their structural density. In this study, the sample was sintered at 600 °C for 2 h. Such heat treatment condition is easy to sinter the TiO_2 nanoparticles in dense. Photocurrent response can not only result from band-to-band transition, but also from sub-band transitions [67]. In principle, there are two kinds of main surface state transitions, population and depopulation. The population transitions can take place from valence bands to the surface states after illumination by photons with sub-bandgap energy. In contrast, the depopulation transitions can occur from the surface

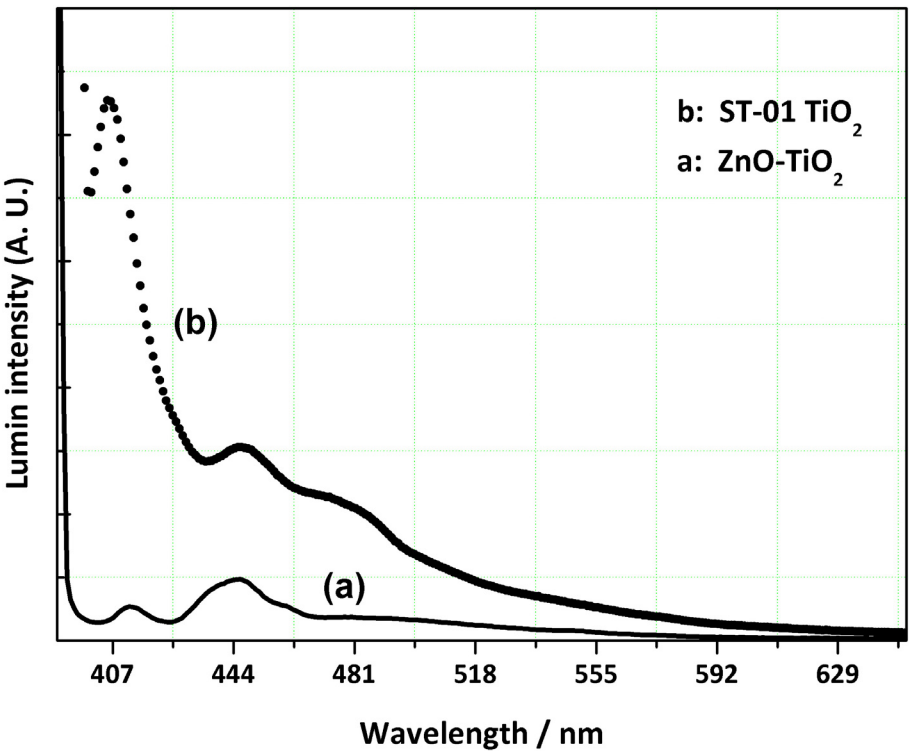

Fig. 4. Emission PL spectra (λ_{ex} = 320 nm) of commercial TiO_2 (ST-01) and ZnO-TiO_2 nanocomposite samples.

states to the conduction bands after illumination by photons with sub-bandgap energy. It can be deduced that the higher is the separation rate of the photoinduced charges, the stronger is the photocurrent signal. The results of photocurrent actions for all the samples are shown in Figure 5, in which the spectra were calibrated with the intensity of the monochromatic incident light. As can be seen, the TiO_2 nanoparticles electrode showed a photocurrent spectrum with the maximum wavelength at around 365 nm corresponding to the band gap of nanocrystalline TiO_2, which was blue-shifted from the band gap of bulk TiO_2 (387 nm, 3.2 eV). In the case of the prepared coupled TiO_2/ZnO nanocomposite, the photocurrent was greatly enhanced with higher photocurrent intensities than that of the monocomponent nanomaterials (ST-01 TiO_2 nanoparticles). The above results imply that the coupling of TiO_2 nanoparticles with ZnO resulted in an improvement in photocurrent generation. Compared to the monocomponent nanomaterials (ST-01 TiO_2 nanoparticles), the larger photocurrent must stem from some combination of more efficient electron injection into the film of coupled TiO_2/ZnO nanocomposites and more efficient electron collection by FTO. The origin of this effect can be multifold. On the one hand, coupling TiO_2 with ZnO could effectively passivate surface recombination sites and act as a radial energy barrier that can repel electrons from the surface of ZnO. On the other hand, electron transport within TiO_2/ZnO composite system could be much faster, and surface fields within composite system could be used to enforce charge separation and thereby ensure that faster transport. Meanwhile, the preserved excellent crystallinity of TiO_2 and ZnO nanoparticles could also enable more efficient electron injection and transport within the coupled TiO_2/ZnO nanocomposite. These results indicated that coupling TiO_2 with ZnO can lead to significant inhibition of recombination probability of photoinduced electron-hole pairs, which in turn results in enhanced photoactivity in the photocatalytic degradation reaction.

Effluents discharged from textile industries are becoming a serious environmental problem because of their unacceptable color, high chemical oxygen demand content, and resistance to chemical and biological degradation. In addition, untreated or partially treated dye wastewaters often contain harmful dyes and toxic aromatic compounds, such as rhodamine B (RhB), which is toxic, mutagenic, and carcinogenic. To test the activity of the prepared catalysts, we chose RhB as a target pollutant in water. The preliminary experiments indicate that the concentration of RhB hardly changed under the visible light irradiation using the commercial TiO_2 (ST-01) catalyst because the wavelength employed is insufficient to activate the pristine anatase-phase TiO_2. Therefore, the photocatalytic activity of ZnO-TiO_2 nanocomposite was evaluated by the photo-induced decomposition of RhB dye

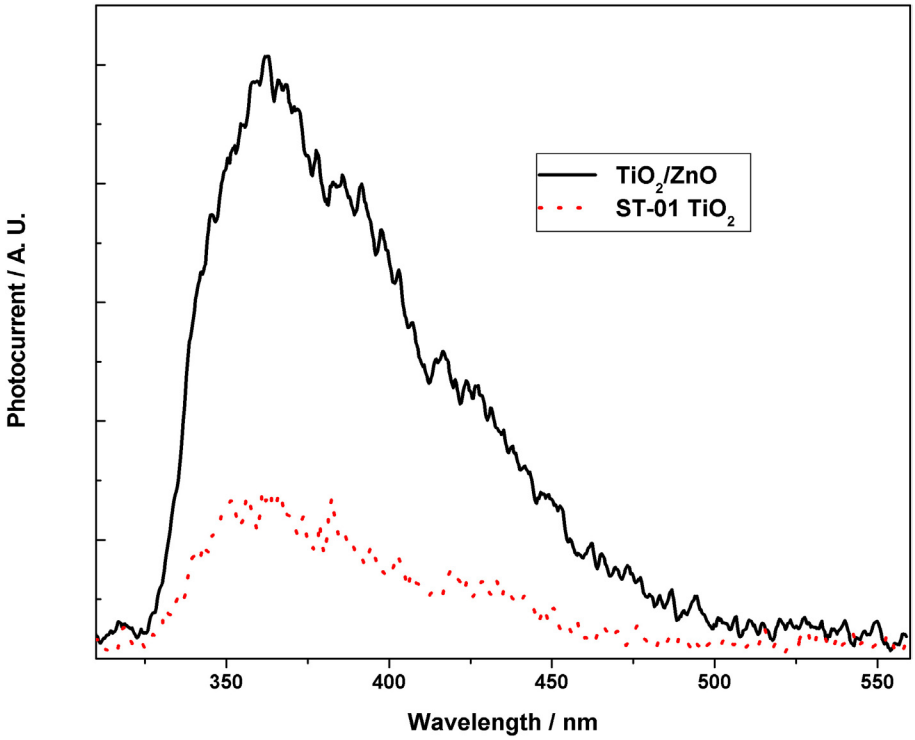

Fig. 5. Photocurrent action spectra of different samples.

under the irradiation of artificial light, and the experiment results are shown in Fig. 6. The temporal evolution of the spectral changes accompanying the photodegradation of RhB over as-prepared coupled ZnO-TiO_2 nanocomposite can be seen. The RhB dye initially showed a major absorption band at 553 nm, while a gradual decrease in absorption with a slight shift of the band to shorter wavelengths was observed with light irradiation through an aqueous RhB solution containing the ZnO-TiO_2 catalyst. During the process of irradiation, the maximum absorption peak shifted gradually from 553 to 498 nm, implying dissociation of ethyl group. From the change of characteristic absorption peak displayed in the graph, under illumination, the dye was de-ethylated in a stepwise manner with the color of the dispersion changing from initial red to pale. De-ethylation of the fully N,N,N',N'-tetraethylrhodamine molecule (i.e., RhB) has the wavelength position of its major absorption band moved toward the blue region, λ_{max}, RhB, 553 nm; N,N,N'-triethylrhodamine, 539 nm; N,N'-diethylrhodamine, 522 nm; N-ethylrhodamine, 510 nm; and Rh, 498 nm. RhB formed Rh after being fully demethylated, and the rest was degraded through destruction of the conjugated structure. Results showed that photodocolorization of chromogenic aromatic ring and dissociation of ethyl occurred simultaneously, and the main reaction at the early stage was the photodecolorization of the chromogenic group. In this case, the dye solution became nearly transparent after 120 min of irradiation, indicates facile removal of the chromophore part of the molecular structure from the RhB dye. During the degradation process, the dye was photodegraded in a stepwise manner with the color of the solution changing from an initial pink to nearly transparent. The above results are in accordance with the photoelectrochemical events. The photocatalytic degradation of MG dye in the presence of the TiO_2/ZnO nanocomposite as catalyst under visible light source irradiations were also investigated. Malachite green (MG) also called basic green 4 or victoria green B, having IUPAC name 4-[(4-dimethylaminophenyl)-phenyl-methyl]-N,Ndimethylaniline with chemical formula $C_{23}H_{25}N_2Cl$, is a green crystal powder with a metallic luster, highly soluble in water and ethanol with blue-green solutions. In Fig. 7, the decay dependency of absorption spectrum on reaction time is given to to reasonably evaluate photocatalytic activities. It is well-known MG solution exhibits a strong absorption peak at 615 nm. Fig. 7 shows the absorption spectra variation of MG vs. irradiation time on the TiO_2/ZnO nanocomposite. The major absorption peaks of MG at around 615 nm diminished gradually under visible light irradiation in the presence of TiO_2/ZnO nanocomposite, and the MG was

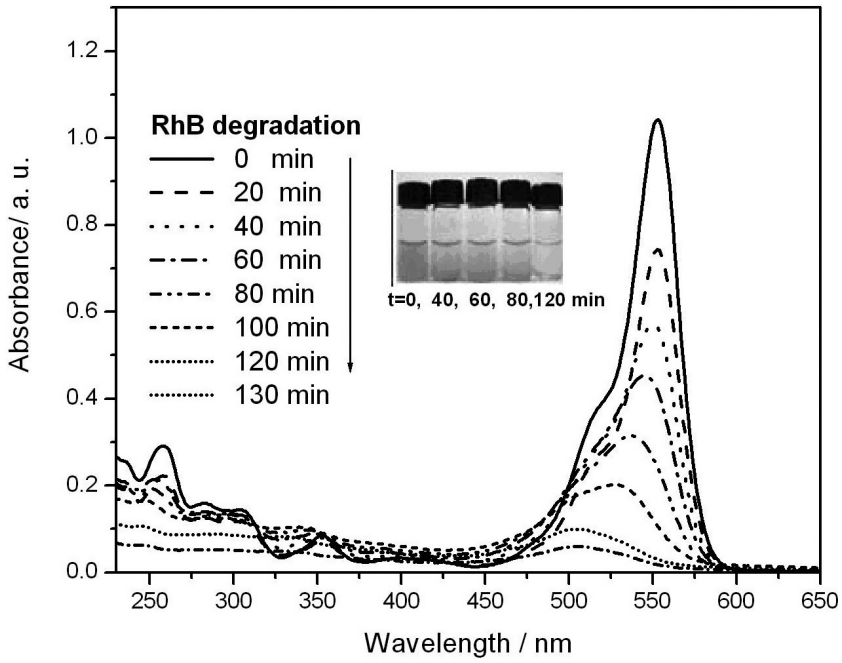

Fig. 6. UV-visible absorption spectral changes of Rhodamine-B aqueous solution over ZnO-TiO_2 nanocomposite catalyst as a function of irradiation time (curves from top to bottom represent different irradiation time: 0, 20, 40, 60, 80, 100, 120 and 130 min, respectively). The inset shows the photograph of the photodegradation of rhB over the ZnO-TiO_2 nanocomposite at different periods.

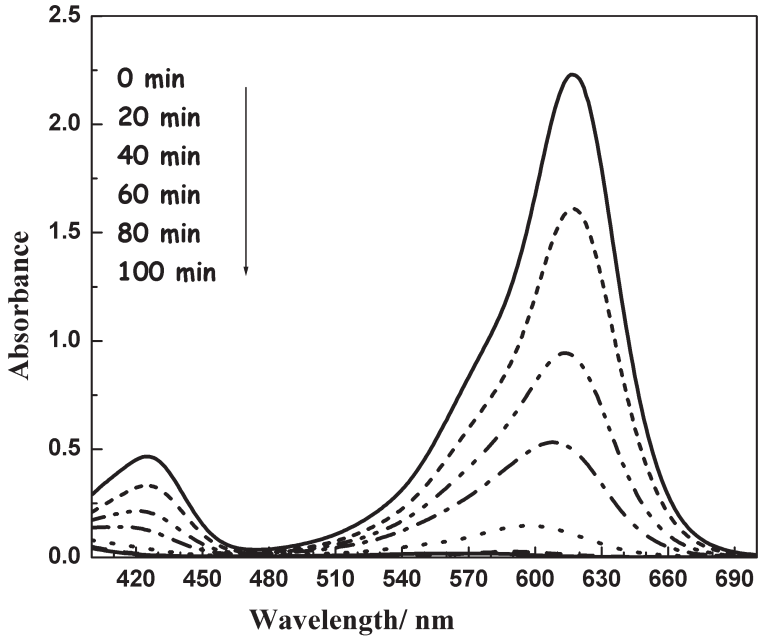

Fig. 7. UV-visible absorption spectral changes of MG aqueous solution over ZnO-TiO_2 nanocomposite catalyst as a function of irradiation time.

almost degraded fully after 80 min. Moreover, the disappearance of another characteristic peak of MG dye around 423 nm also take place with the increase of time, which indicates that the MG dye can be effectively decolorizated utilizing TiO_2/ZnO nanocomposite. The decolorization efficiency of the MG dye is around 97 % after 100 min under visible light irradiation. The mechanism of the charge separation and photocatalytic reaction for the as-prepared ZnO-TiO_2 nanocomposite photocatalyst can be illustrated as follows. According to the literature report, ZnO has the same band gap energy of anatase TiO_2 (3.2 eV) and similar electronic properties, but it has CB energy more positive than that of anatase TiO_2. Upon light-activation, the electron will transfer from the CB of ZnO to that of anatase TiO_2. However, the energy position values show that the rutile TiO_2 still have CB energy more negative than that of anatase TiO_2 [68—70]. Therefore, the electrons accumulated on the CB of anatase TiO_2 will automatically drifted to the CB of rutile TiO_2 due to the difference in the energy band position. Thus, there existed a cooperative relationship between ZnO, anatase and rutile. A proper reaction mechanism for ZnO-TiO_2 nanocomposite photocatalyst can be proposed, that is, the VB of ZnO is higher than that of anatase, and the CB of anatase is higher than that of rutile. In the ZnO-TiO_2 nanocomposite, the electrons and holes are generated on the anatase surface upon activation. Then the generated electrons could transfer from the CB of light-activated anatase to that of rutile. Conversely, the generated holes could move into the VB of ZnO from anatase. Such a coupled effect among ZnO-anatase/rutile multiple-component interface could retard the occurrence of recombination between electrons and holes [71—76]. This efficient charge separation prolongs the lifetime of the charge carriers and enhances the photocatalytic efficiency of ZnO-TiO_2 nanocomposite in comparison with to pure TiO_2 photocatalyst. As a result, the photocatalytic oxidation activity of ZnO-TiO_2 nanocomposite was improved greatly.

Conclusions

In summary, ZnO-TiO_2 nanocomposite catalyst was synthesized via sol-gel process. In addition to the formation of $ZnTiO_3$ crystallites, intermingled crystallites including anatase or rutile TiO_2 and wurtzite ZnO were predominantly formed at calcinations temperature of 600 °C. The prepared ZnO-TiO_2 nanocomposite sample shows a red-shift as compared to commercial TiO_2 (ST-01) sample in UV-visible spectrophotometry and are active in visible light region as well as enhanced light absorption for the photocatalytic degradation of aqueous RhB and MG dye. The charge separation of electrons and holes was promoted and the recombination of electron-hole pairs was restrained because of the coupling effect of mixed-phase TiO_2 and single-phase ZnO in the composite nanoparticles. As a consequence, the ZnO-TiO_2 nanocomposite showed much higher photocatalytic efficiency than untreated TiO_2 in degrading Rhodamine-B

molecules in water. This study shows that coupling a photocatalyst with high recombination rate to a suitable material will enhance its activity and the as-prepared ZnO-TiO_2 nanocomposite can be used as a highly efficient photocatalyst for promising applications in the treatment of organic-polluted water, and have potential applications in pollutant removal under natural solar light.

Acknowledgments

This work was supported by the Natural Science Foundation of Hubei Province of China (Project no: 2011CDB148) and the Fundamental Research Funds for the Central Universities (Project no: 2013QC026).

References

1. Kochuveedu ST, Jang YH, Kim DH (2013) Chem Soc Rev 42: 8467–8493.
2. Wang YN, Deng KJ, Zhang LZ (2011) J Phys Chem C 115: 14300–14308.
3. Xu H, Zhang LZ (2010) J Phys Chem C 114: 11534–11541.
4. Zhang JW, Zhu PL, Li JH, Chen JM, Wu ZS, Zhang ZJ (2009) Cryst Growth Des 9: 2329–2334.
5. Zhang LW, Zhu YF (2012) Catal Sci Technol 2: 694–706.
6. Zhang HC, Huang H, Ming H, Li HT, Zhang LL, Liu Y, Kang ZH (2012) J Mater Chem 22: 10501–10506.
7. Zhang SW, Xu WQ, Zeng MY, Li JX, Xu JZ, Wang XK (2013) Dalton Trans 42: 13417–13424.
8. Zhang J, Xi JH, Ji ZG (2012) J Mater Chem 22: 17700–17708.
9. Zhang SW, Li JX, Niu HH, Xu WQ, Xu JZ, Hu WP, Wang XK (2013) ChemPlusChem 78: 192–199.
10. Zhang K, Jing DW, Chen QY, Guo LJ (2010) Int J Hydrogen Energy 35: 2048–2057.
11. Guo YD, Zhang GK, Liu J, Zhang YL (2013) RSC Adv 3: 2963–2970.
12. Guo YD, Zhang GK, Gan HH, Zhang YL (2012) Dalton Trans 41: 12697–12703.
13. Wan Z, Zhang GK, Wang JT, Zhang YL (2013) RSC Adv 3: 19617–19623.
14. Zhang J, Qiao SZ, Qi LF, Yu JG (2013) Phys Chem Chem Phys15: 12088–12094.
15. Zhang J, Liu SW, Yu JG, Jaroniec M (2011) J Mater Chem 21: 14655–14662.
16. Zhang J, Zhang YP, Lei YK, Pan CX (2011) Catal Sci Technol 1: 273–278.
17. Zhang LW, Dillert R, Bahnemann D, Vormoor M (2012) Energy Environ Sci 5: 7491–7507.
18. Yu JG, Zhang J (2010) Dalton Trans 39: 5860–5867.
19. Sajjad S, Leghari SAK, Zhang JL (2013) RSC Adv 3: 12678–12687.
20. Xiao X, Zhang WD (2011) RSC Adv1: 1099–1105.
21. Ge SX, Jia HM, Zhao HX, Zheng Z, Zhang LZ (2010) J Mater Chem 20: 3052–3058.
22. Liu J, Zhang GK, Yu JC, Guo YD (2013) Dalton Trans 42: 5092–5099.
23. Yu JG, Zhang J, Jaroniec M (2010) Green Chem 12: 1611–1614.
24. Song SY, Gao W, Wang X, Li XY, Liu DP, Xing Y, Zhang HJ (2012) Dalton Trans 41: 10472–10476.
25. Xiao X, Zhang WD (2010) J Mater Chem 20: 5866–5870.
26. Zhang GK, Shen X, Yang YQ (2011) J Phys Chem C 115: 7145–7152.
27. Ge SX, Wang BB, Lin J, Zhang LZ (2013) CrystEngComm 15: 721–728.
28. Zhang ZZ, Luo ZS, Yang ZP, Zhang SY, Zhang Y, Zhou Y, Wang XX, Fu XZ (2013) RSC Adv 3: 7215–7218.
29. Zhang YL, Deng LJ, Zhang GK, Gan HH (2011) Colloid Surface A 384: 137–144.
30. Zhang YL, Wang DJ, Zhang GK (2011) Chem Eng J 173: 1–10.
31. Zhang YL, Guo YD, Zhang GK, Gao YY (2011) Appl Clay Sci 51: 335–340.
32. Zhang L, Tian BZ, Chen F, Zhang JL (2012) Int J Hydrogen Energ 37: 17060–17067.
33. Tian BZ, Li CZ, Zhang JL (2012) Chem Eng J 191: 402–409.
34. Jiao YC, Chen F, Zhao B, Yang HY, Zhang JL (2012) Colloid Surface A 402: 66–71.
35. Wu YM, Xing MY, Zhang JL (2011) J Hazard Mater 192: 368–373.
36. Zhang MY, Shao CL, Zhang P, Su CY, Zhang X, Liang PP, Sun YY, Liu YC (2012) J Hazard Mater 225–226: 155–163.
37. Zhang J, Su YJ, Wei H, Wang J, Zhang C, Zhao J, Yang Z, Xu MJ, Zhang LL, Zhang YF (2013) Mater Lett 107: 251–254.
38. Shi YF, Chen F, Zhang JL (2013) Appl Surf Sci 265: 912–918.
39. Zhang YH, Tang ZR, Fu XZ, Xu YJ (2010) ACS Nano 4: 7303–7314.
40. Zeng CY, Tian BZ, Zhang JL (2013) J Colloid Interf Sci 405: 17–21.
41. Chen CH, Liang YH, Zhang WD (2010) J Alloy Compd 501: 168–172.
42. Zhang GK, Li M, Yu SJ, Zhang SM, Huang BB, Yu JG (2010) J Colloid Interf Sci 345: 467–473.
43. Zhang YL, Gan HH, Zhang GK (2011) Chem Eng J 172: 936–943.
44. Zhang LY, Yin LW, Wang CX, Lun N, Qi YX (2010) ACS Appl Mater Interfaces 2: 1769–1773.
45. Zhang YC, Li J, Zhang M, Dionysiou DD (2011) Environ Sci Technol 45: 9324–9331.
46. Wang LZ, Jiang L, Xu CC, Zhang JL (2012) J Phys Chem C 116: 16454–16460.
47. Zhang J, Yu JG, Zhang YM, Li Q, Gong JR (2011) Nano Lett 11: 4774–4779.
48. Ai ZH, Zhang LZ, Lee SC (2010) J Phys Chem C 114: 18594–18600.
49. Zhang J, Yu JG, Jaroniec M, Gong JR (2012) Nano Lett 12: 4584–4589.
50. Zhang JY, Wang YH, Zhang J, Lin Z, Huang F, Yu JG (2013) ACS Appl Mater Interfaces 5: 1031–1037.
51. Zhang WD, Zhang Q, Dong F (2013) Ind Eng Chem Res 52: 6740–6746.
52. Dong RF, Tian BZ, Zeng CY, Li TY, Wang TT, Zhang JL (2013) J Phys Chem C 117: 213–220.
53. Zhang J, Pan CX, Fang PF, Wei JH, Xiong R (2010) ACS Appl Mater Interfaces 2: 1173–1176.
54. Su K, Ai ZH, Zhang LZ (2012) J Phys Chem C 116: 17118–17123.

55. Zhang JW, Zhang M, Jin ZS, Wang JJ, Zhang ZJ (2012) Appl Surf Sci 258: 3991–3999.
56. Zhang LW, Man Y, Zhu YF (2011) ACS Catal 1: 841–848.
57. Jiang J, Zhang X, Sun PB, Zhang LZ (2011) J Phys Chem C 115: 20555–20564.
58. Zhang H, Lv XJ, Li YM, Wang Y, Li JH (2010) ACS Nano 4: 380–386.
59. Zhang SM, Chen YY, Yu Y, Wu HH, Wang SR, Zhu BL, Huang WP, Wu SH (2008) J Nanopart Res 10: 871–875.
60. Zhang X, Zhang LZ, Xie TF, Wang DJ (2009) J Phys Chem C 113: 7371–7378.
61. Zhang X, Zhang LZ (2010) J Phys Chem C 114: 18198–18206.
62. Zhang H, Zhu YF (2010) J Phys Chem C 114: 5822–5826.
63. Zhang YP, Pan CX (2011) J Mater Sci 46: 2622–2626.
64. Zhang JL, Wu YM, Xing MY, Leghari SAK, Sajjad S (2010) Energy Environ. Sci 3: 715–726.
65. Zhang YA, Fan HQ, Li MM, Tian HL (2013) Dalton Trans 42: 13172–13178.
66. Wan Z, Zhang GK, Wang JT, Zhang YL (2013) RSC Adv 3: 19617–19623.
67. Riaz N, Chong FK, Dutta BK, Man ZB, Khan MS, Nurlaela E (2012) Chem Eng J 185-186: 108–119.
68. Zhang DF (2013) Acta Chim Slov 6: 141–149.
69. Feng CX, Jin ZS, Zhang JW, Wu ZS, Zhang ZJ (2010) Photochem Photobiol 86: 1222–1229.
70. Jiang J, Zhang LZ (2011) Chem Eur J 17: 3710–3717.
71. Jiang J, Li H, Zhang LZ (2012) Chem Eur J 18: 6360–6369.
72. Zhang YP, Li CZ, Pan CX (2012) J Am Ceram Soc 95: 2951–2956.
73. Xu YS, Zhang WD (2013) Chemcatchem 5: 2343–2351.
74. Sajjad S, Leghari SAK, Chen F, Zhang JL (2010) Chem Eur J 16: 13795–13804
75. Yu H, Tian BZ, Zhang JL (2011) Chem Eur J 17: 5499–5502.
76. Zhang YP, Fei LF, Jiang XD, Pan CX, Wang Y (2011) J Am Ceram Soc 94: 4157–4161.